Optimal site selection for Choutuppal geomagnetic observatory, based on geophysical evidences

Divyanshu Dwivedi[1], Sneh Yadav[2], Kusumita Arora[1], Rakesh Murteli[1], Alok Taori[3]
[1]Geomagnetism, CSIR-National Geophysical Research Institute, India
[2]Kurukshetra University, India
[3]National Remote Sensing Centre, India
Correspondence: Divyanshu Dwivedi; email id: ddwivedigp@gmail.com

Abstract

The phases of development of the Choutuppal magnetic observatory over last 15 years has enabled the effects of the natural environment like groundwater changes and lightning activity on the magnetic data to be evaluated. A high resolution survey of total field anomalies led to the construction of a 3D model of the shallow surface. Constrained by conductivity depth slices from previous electrical resistivity tomography and electrical vertical resistivity imaging surveys, the distribution of sandy regolith, saprolite, and granitic layers in the shallow subsurface are delineated. The pattern of lightning strikes in a 10 km area around the observatory are correlated to modulations and disruptions in the magnetic data. The analysis as a whole provides information for selecting a location to install a secondary variometer room by taking into account topography, lightning effect, soil resistivity, low magnetic anomaly and distance from the recharge pond, which can produce continuous data of higher quality and consistency than at present.

Keywords: Choutuppal observatory, Magnetic anomaly, Spectral analysis, Lightning data

1. Introduction:

The Choutuppal (CPL) geo-electric observatory (Geographic coordinates: 78.920E, 17.290N; Geomagnetic coordinates: 149.24E, 7.47N) of CSIR-NGRI was established near Choutuppal town in the Nalgonda district, approximately 60 km southeast of Hyderabad city, Telangana state (Sanker Narayan, 1964). The region primarily comprises granite and gneissic formations. These rocks are part of the Peninsular Gneissic Complex, which is one of the oldest geological formations in India, dating back to the Archean era. The weathering of the granitic and gneissic rocks has led to the formation of red and lateritic soils. The granitic formation is encroached locally by discontinuities such as dikes or quartz reefs but these are not present on the site (Guihéneuf et al., 2014). The area around the CPL observatory mainly consists of alkali feldspar granite (Figure 1a). The regional geology of resistive granitic basement rocks, uniform soil cover, arid vegetation, and gentle topography for effective drainage of runoff water during rainy seasons were assessed to be suitable for geo-electric measurements (Sanker Narayan et al., 1967; Sarma et al., 1969). Below the surface, shallow drillings revealed: 1) A sandy regolith layer 0-2 m thick which is made up of sandy-clay of quartz grains, 2) A laminated saprolite layer of variable thickness of 10 - 15 m derived from in-situ weathering of granite, 3) A 15-20 m thick layer of fissured granite, where weathered granite and some clay partially fill the fissures. The effective porosity of this layer is very low and mainly due to the fissure zones (Dewandel et al., 2006; 2012).

The geo-electric measurements at CPL were based on orthogonal 500 m electric dipoles and magnetic pulsations were measured with solid core induction coils. Hourly values of the magnetic variation and analysis of equatorial magnetic pulsations were

reported from CPL (CSIR NGRI report, 1972). These hourly values are published in the Indian magnetic data volumes and uploaded to WDC Kyoto (Svendsen et al., 1990). Figure 1b shows the 105-acre, star-shaped campus of CSIR-NGRI located in Choutuppal, along with the marked locations of the Primary Variometer (PVR) and Absolute (ABS) rooms. One high magnetic anomaly is present at the eastern part of the campus. In the rest of the area, the total range is ~ 80 nT. The surface topography is least in the east and north and higher is the west and southern part of the campus. Several shallow boreholes drilled in the northern end are used for hydrogeological studies in fractured hard rock terrains. These studies monitored the nature of the granitic basement rocks, local hydrogeology, and managed aquifer recharge (MAR) within the CPL observatory, through a large, shallow lake in the eastern quadrant of the campus.

Geo-electric measurements on this campus were discontinued in 1982, but when the Metro Rail project in the vicinity of the HYB magnetic observatory in Hyderabad appeared to threaten its existence in 2010, the Choutuppal campus was re-visited for re-location possibilities of HYB. This work summarizes the different situations, which affect the operation of a low latitude magnetic observatory, some mitigation measures and some unanswered questions.

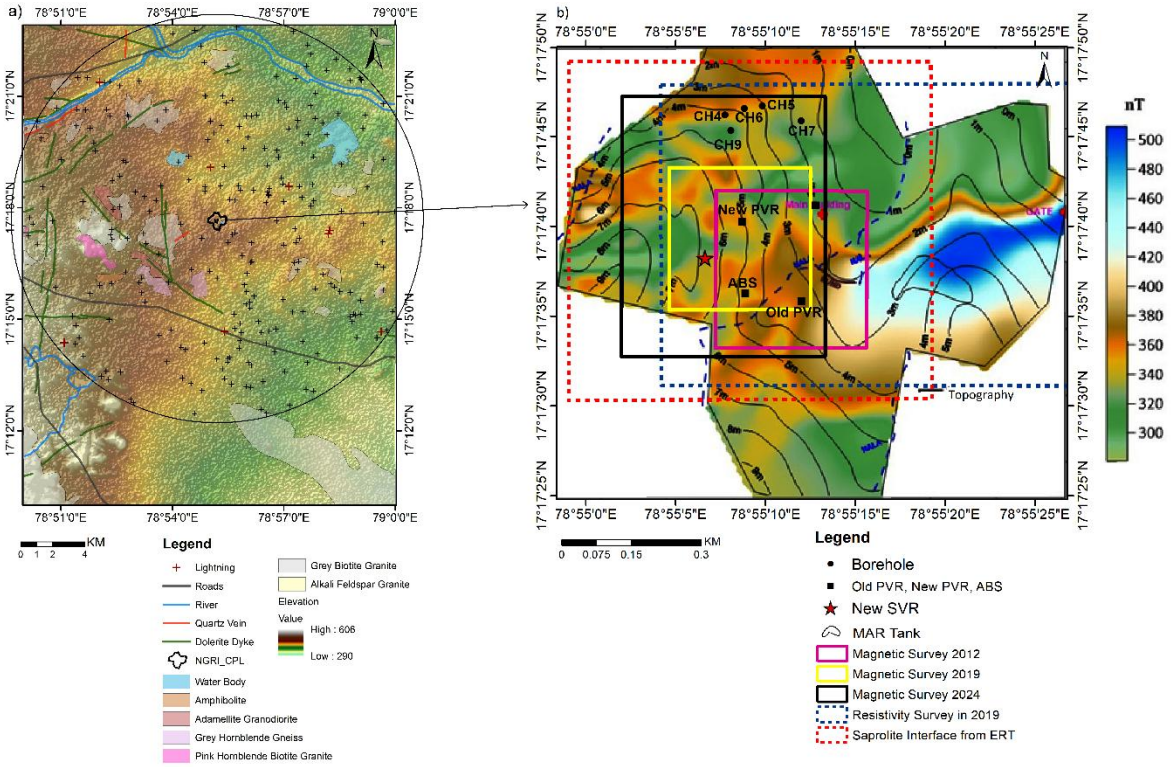

Figure 1: a) The geological map shows the area around the CSIR-NGRI-CPL observatory superimposed over topography. '+' symbols show lightning locations within a 10 km radius (circle mark) from January 2022 to August 2022 with maximum intensity 60480 amp, b) The magnetic anomaly map (after Sanker Narayan et al., 1967) is superimposed on local elevation. The locations of the magnetic and electric surveys are marked by solid and dashed rectangles. PVR=Primary variometer room, ABS= Absolute room, SVR= Secondary variometer room, MAR = managed aquifer recharge.

2. First phase of CPL Magnetic Observatory:

i) Survey of magnetic data and building CPL Observatory

Prior to establishing the observatory buildings, a magnetic survey was conducted in November 2012 over an area of 200 m x 200 m with 20 m intervals, between the Main Building and the southern side of the campus, marked by pink rectangle in Figure 1b, which had the smallest anomalies as per the earlier survey. This area was sufficiently far away from the boundary of the campus to ensure that local activities outside the campus may not have significant contribution to the measurements. The total

magnetic anomaly range (Figure 2) was ~ 150nT with changes in magnetic field within ~20 nT around proposed locations of the old PVR and ABS rooms.

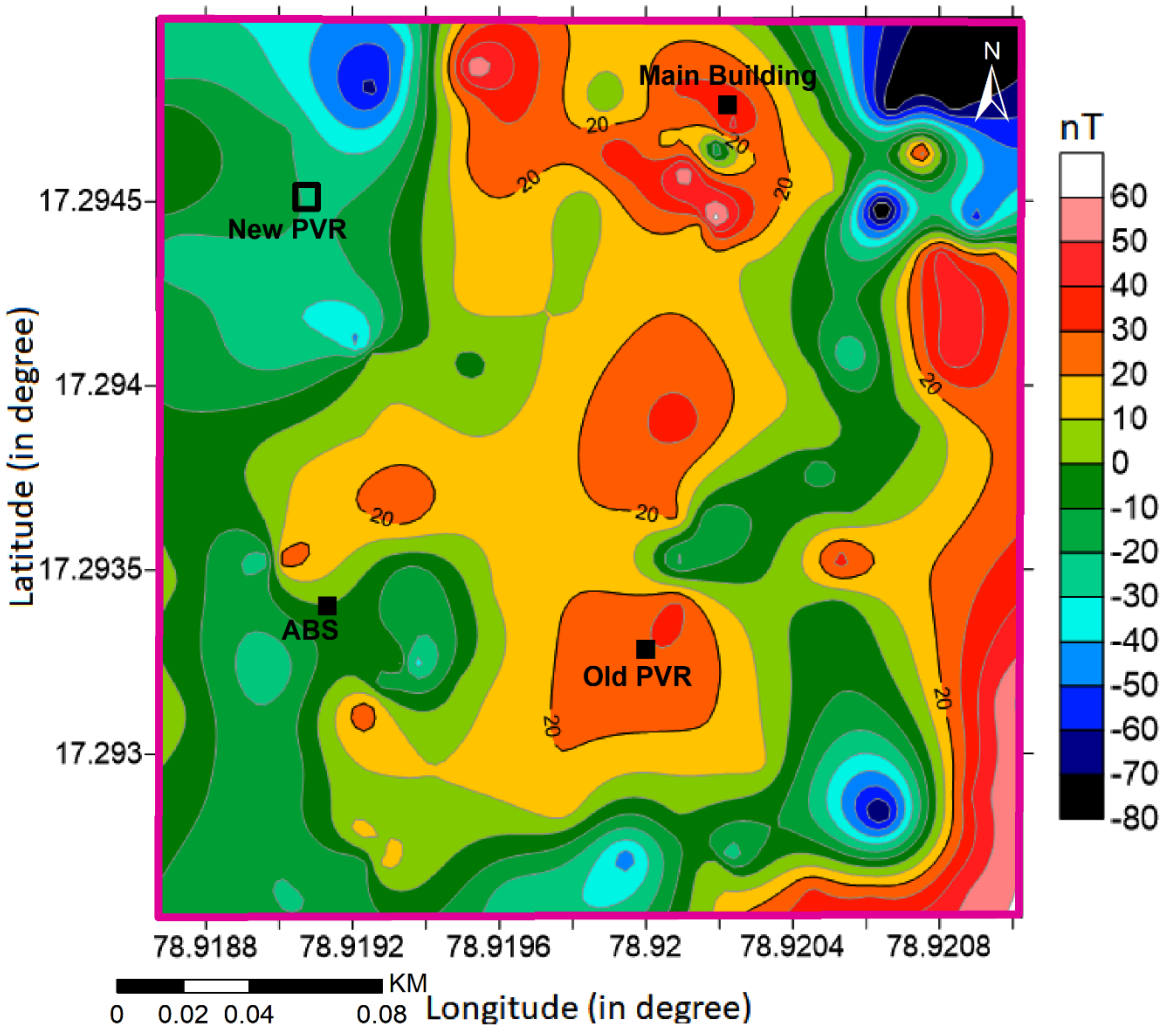

Figure 2: Magnetic anomaly plot of the survey region in 2012. Black box is the marked location for the New PVR, built in 2019-2020.

In this central location the surface topography is low and a shallow water channel (nalla) flows SE-NW through the area between the Old PVR and ABS. The Old PVR construction (with double walled, 3.5 m underground vault) started in the June 2013 using non-magnetic sandstone. The ABS room was constructed on slightly elevated ground with two pillars inside and four pillars outside. In April 2014, the CPL observatory was commissioned, equipped with tri-axial fluxgate magnetometer and

Zeiss single axis fluxgate theodolite for Declination-Inclination measurements. The XVII IAGA Observatory Workshop was held on these premises in October 2014 with 93 international participants from 33 countries. The definitive data from CPL is published at INTERMAGNET, 2015 onwards.

ii) Hydrogeological Park and managed aquifer recharge:

The region of CPL Observatory has a semi-arid climate with an average annual maximum temperatures ranging as 28°C - 45°C. The mean annual rainfall is around 751 mm, which ranges from 2 mm in February to 171 mm in July. Water levels are highly variable depending on the monsoon and usually range between 2 and 26 m (meters below ground surface). Water level measurements at the northern part of the Choutuppal campus has been monitored since 1999 in two dozen boreholes, some of them are marked in Figure 1b, by the Indo-French Center for Groundwater Research (IFCGR) (Maréchal et al, 2018) to study the hydrodynamic properties and associated hydrological processes in crystalline aquifers. As part of a governmental scheme of strengthening groundwater through recharge state-wise MAR projects, an infiltration basin was dug in Choutuppal (marked in black outline as MAR in Figure 1b) in 2015 to meet the demands of farmers in the area facing water scarcity. The basin has dimensions of 120 m × 40 m, with a depth of about 2 m, effectively removing the regolith layer and extending into the saprolite. The basin is mainly supplied by a canal which diverts water from the Musi River (Nicolas et al., 2019; Maurya et al., 2021). Nicolas et al (2019) has shown that intra-seasonal groundwater fluctuations have only moderate response to rainfall patterns, which could be due to usage trends as well as hydraulic permittivity parameters. After the MAR basin filling, groundwater levels rose by 6 m in one year. Figure 3a shows the water level changes of five boreholes (CH5,

CH6, CH4, CH7, and CH9) before and after monsoon from 2011 to 2023 with a data gap during 2021-22. While it is clear that most of the time water level lies at intermediate depth of ~ 10 to 30 m, individually, CH5 and CH7 show the least seasonal fluctuations over the years, CH6, CH4 and CH9 show variations of 20 m or more; possibly very local fracture properties facilitate vertical flow of water. Starting from April 2017, the water levels in the boreholes rose significantly, coming almost to surface in September 2017 and reducing a little by July 2018. In December 2023, the water levels recorded are nearly similar to that of September 2017. It can be inferred that sustained water in the MAR basin has allowed the shallow aquifers to be permanently recharged. In September 2017, the rainfall of the monsoon combined with prevalent saturated condition led to the flooding of the Old PVR vault (Figure 3c). The water level receded by a few metres the following summer but did not fall to earlier levels. While this was good news for recharge, the Old PVR was now unusable.

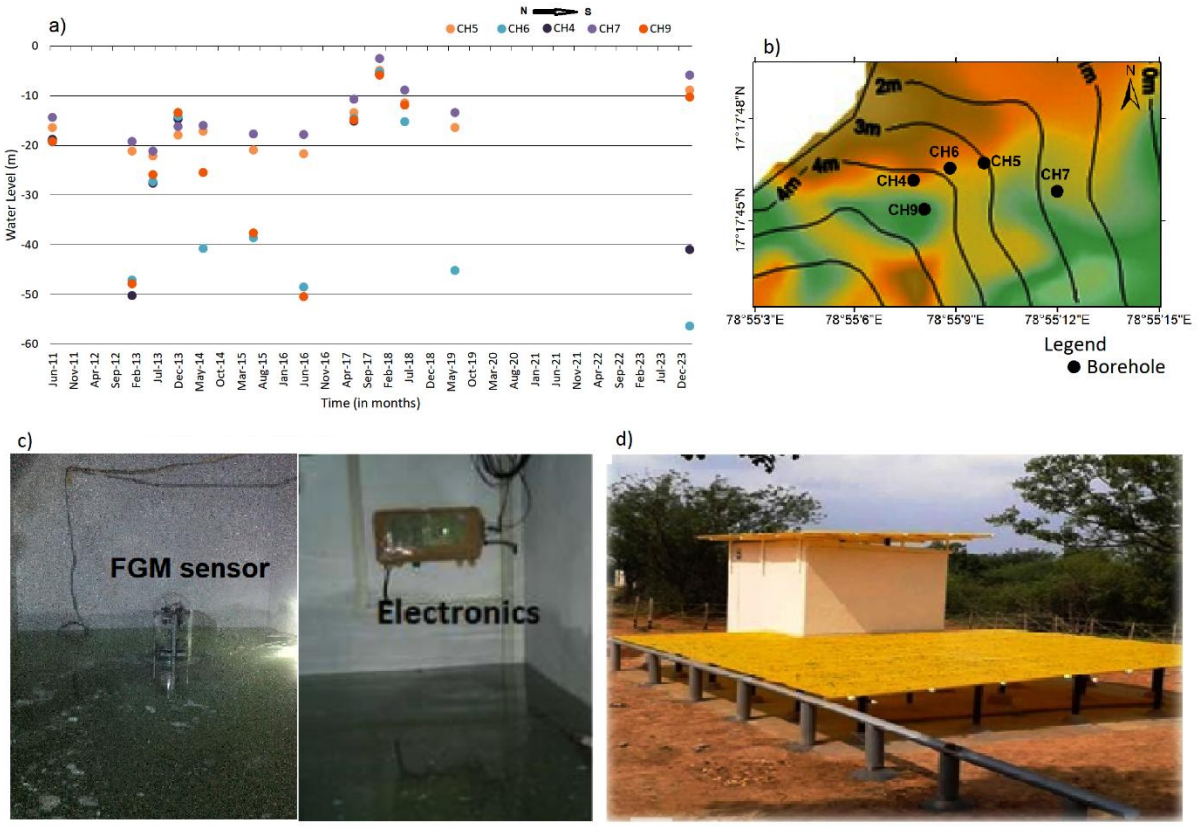

Figure 3: a) Fluctuations of water level in a few boreholes in the north of Choutuppal campus, b) location of boreholes in the map, c) the submerged vault in September 2017, d) the outside view of the old PVR.

3. Second phase of CPL Magnetic Observatory:

i) Survey and commissioning of new PVR

With the need for a new variometer building, a fresh survey was conducted in May 2019 using GSM19 Overhauser magnetometers, marked by the yellow rectangle in Figure 1b. This area was some tens of meter west of the earlier survey location, still central to the campus, on ground which is about 2-3 m higher, which could avoid the shallow groundwater conditions. This total field magnetic survey was carried out during six geomagnetic quiet days in May 2019 over a 240 × 240 square meter area with 10 m spacing. The magnetic anomaly of the region shows total amplitude variation of ~300nT (Figure 4a) with ~10nT anomaly north of the ABS room; the proposed location is marked as New PVR in Figure 4a. This time a raised building with double walls and double roof was constructed of non-magnetic limestone to ensure no groundwater incursion issues for the foreseeable future (Figure 4b). The New PVR was commissioned in January 2021.

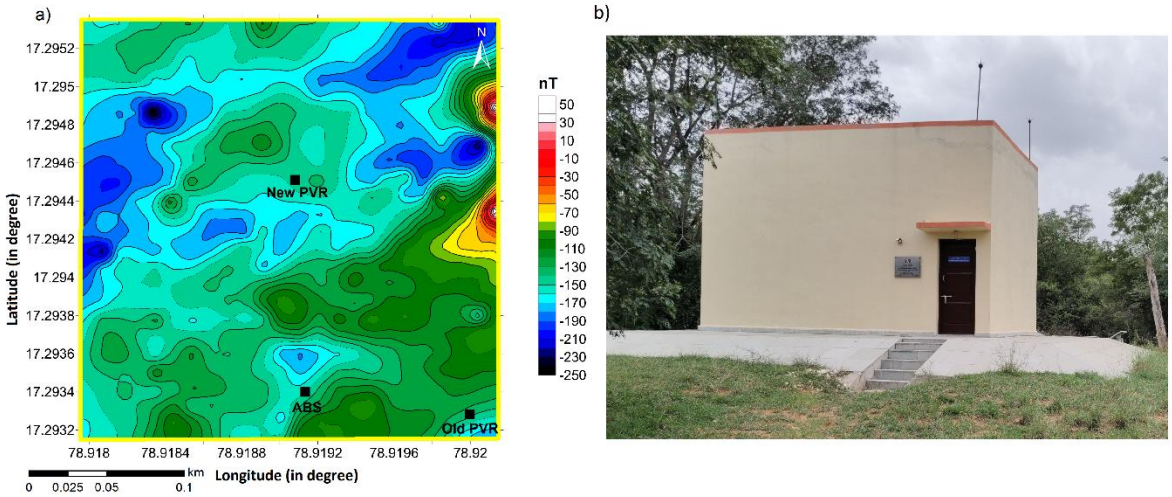

Figure 4: a) Magnetic anomaly plot of the survey region in 2019, b) New PVR building inaugurated in January 2021.

Recurrent malfunctions of the electronics (2-3 times a month) of the digital fluxgate magnetometer (DFM) recording electronics were noticed in second half of 2021 and 2022, a new phenomenon. After rounds of thorough inspections, it was suspected that lightning activity in the vicinity of the Choutuppal campus was causing the damage inspite of installation of 6 lightning arrester rods and 4 earthing pits. Being an open ground with no tall obstructions, the lightning activity in this area was found to be more frequent than around HYB observatory in Hyderabad. The earthing pits and lightning arrester system were strengthened further but only marginally countered the effects on the electronics.

ii) Lightning activity patterns around CPL Observatory and effects on data

ISRO-National Remote Sensing Center (NRSC) has a network of 46 radio frequency lightning detection sensors, covering the entire part of the India (shown in Figure 5a). The Lightning detection sensor network monitors the cloud to ground lightning occurrences by virtue of emitted waves in the 5 Hz - 30 MHz range and geolocation is calculated using the time of arrival method. The detection range is upto 800 km with more than 98% confidence within 300 km range, with 50% overlap to maintain high geo-location accuracy of lightning occurrences (Taori et al., 2022; 2023). We have examined the lightning data in a radius of 10 km around CPL observatory, marked as + in Figure 1a. Figure 5b shows the shows the occurrence frequency of lightning over the months from January to August 2022; + symbols denote the instances when the lightning caused damage in the fluxgate electronics. Figure 5b shows that substantial

lower intensity lightning activities are recorded during January, April, May and June. Surprisingly July had no lightning in the area in 2022, in August, the higher intensity lightning was more numerous. Two instances of failure of the instrument electronics occurred during the higher intensity lightning of April and August, whereas a disturbance of May was associated with lower amplitude lightning, discussed in next section.

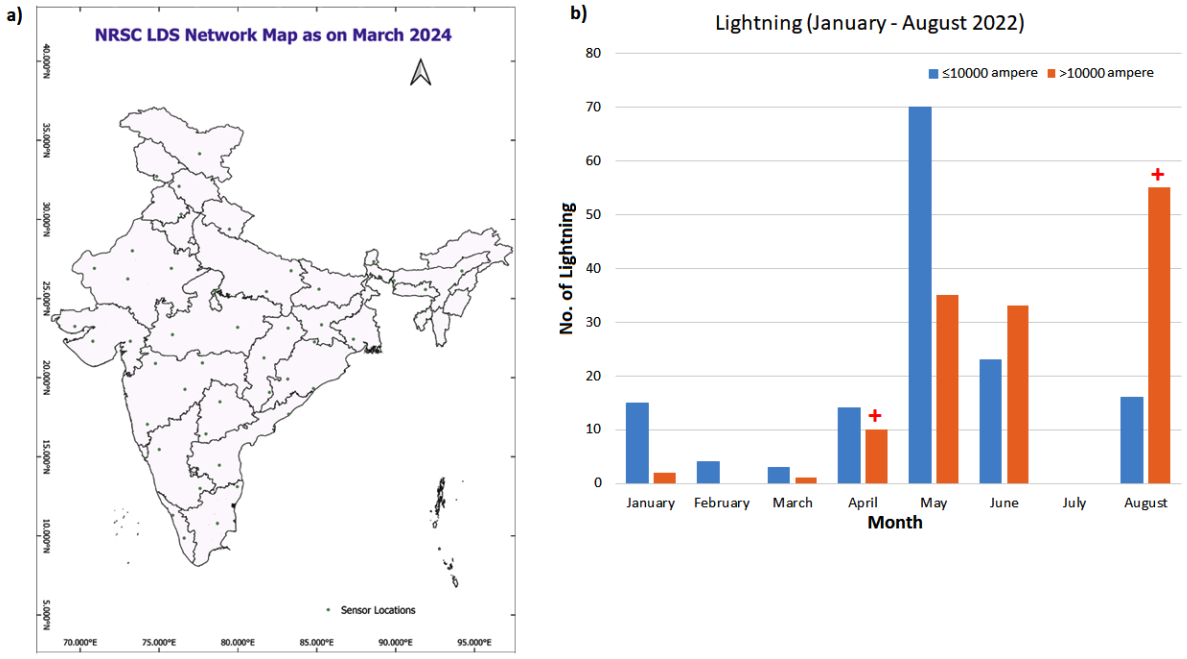

Figure 5: a) Map of lightning sensors in India, b) Distribution of low and high intensity lightning occurrences during January to August 2022.

Examination of the H (horizontal), D (declination), and Z (vertical) components of 1-sec data in LT (local time) for 04th May, 2022 data from the new PVR shows continuous spikes from 7- 8.2 LT in all the components, followed by a shift of ~ 70, 20 and 150 nT in H, D and Z respectively (Figure 6a). After rebooting the instrument, the data came back to its normal range. Comparison with lightning data established that this disturbance was due to lightning effect (correlated red mark). It is noticed that at the time of 7.94 LT hour there was shift in the data which correlate with the lightening

intensity of 8879 and 14243 ampere at the same time, which strike the ground within 10 km radius of CPL campus.

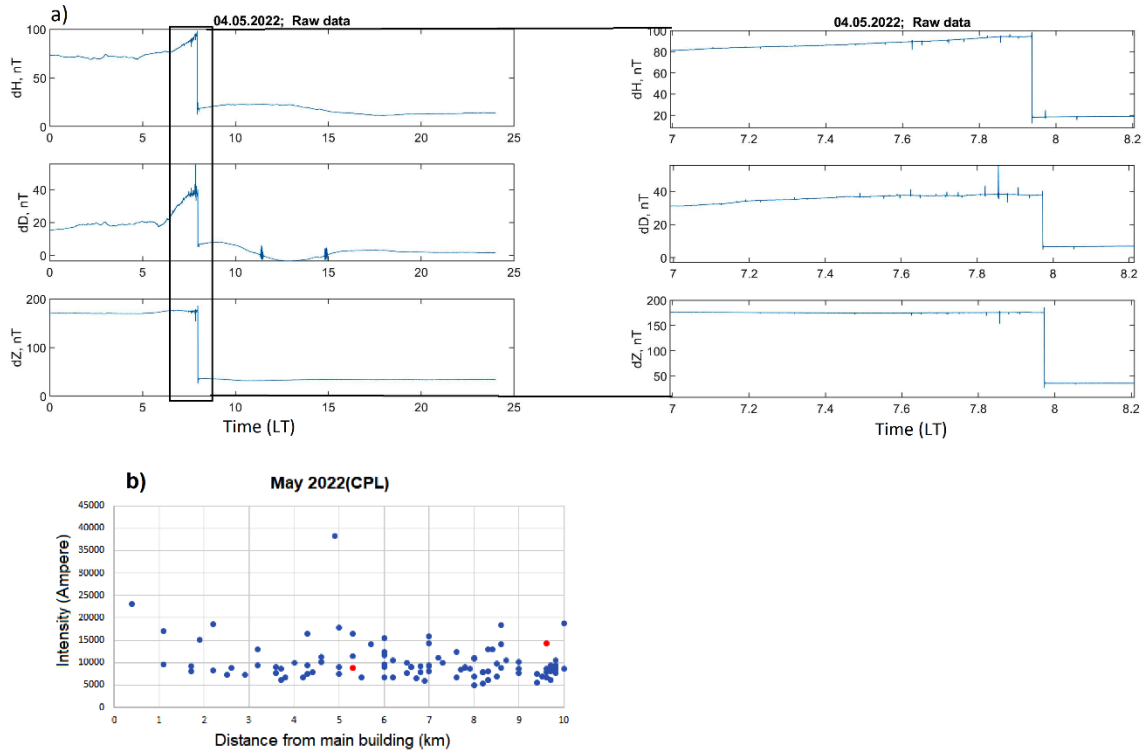

Figure 6: Raw data (H, D, Z component) plot for a) 04th May, 2022 at the new PVR, b) plot of lightning intensity (in ampere) with distance (in km) from main building.

Further, we examined the H, D, Z components of 1-sec data in LT for the 30th April and 26th May, 2017 data from the Old PVR, on days which had some weather activities. From the data, it is clear that there were no shifts in the data, but some continuous spikes were observed from 18.0 -18.8 LT (Figure 7). The spikes are more prominent in the Z component (>0.5nT). Though lighting data was not available in this duration, the general conditions lead us to believe that these minor signatures were lightning induced.

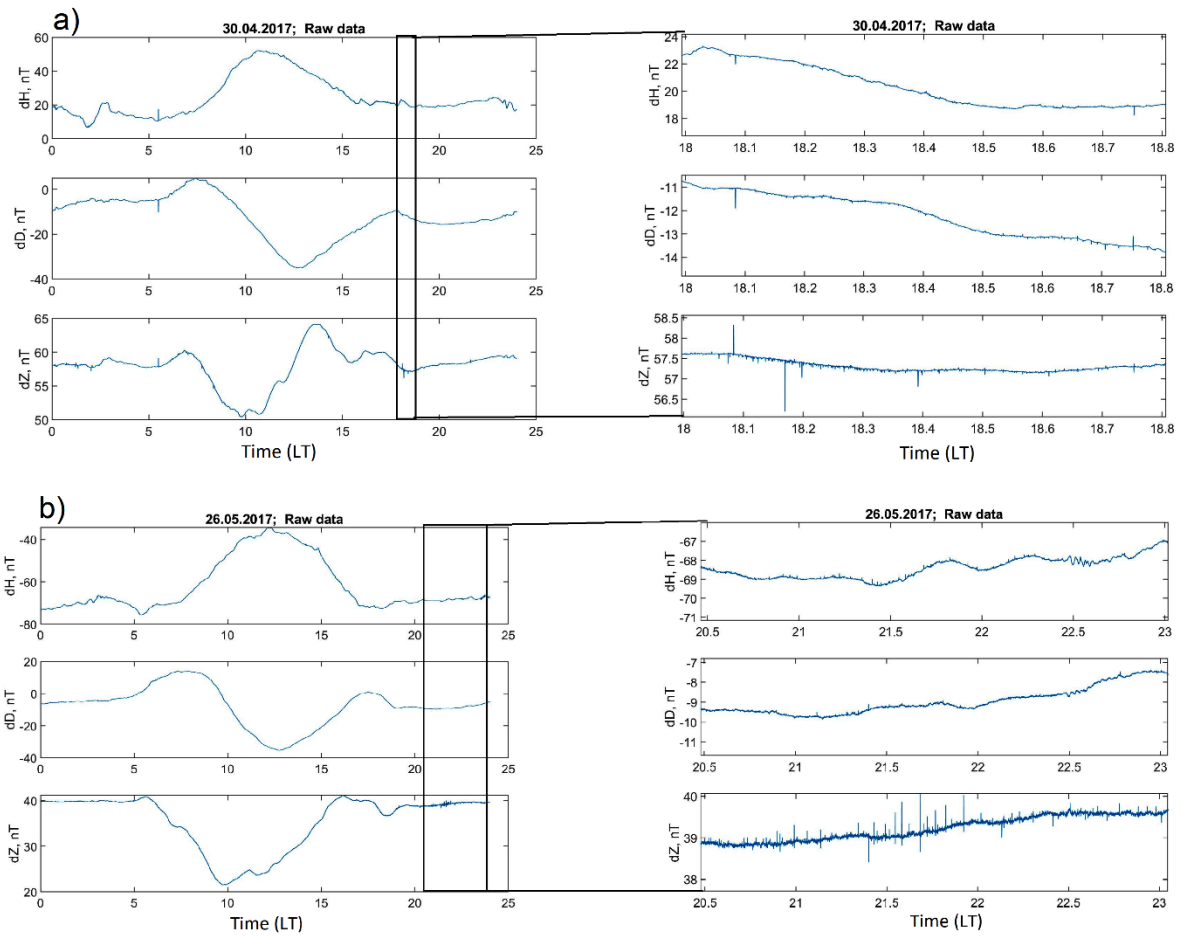

Figure 7: Raw data (H, D, Z component) plot for a) 30th April, b) 26th May, 2017 at the old PVR.

Table 1 provides examples of the amplitudes of the disturbances recorded in data vis-à-vis the light intensities and distance from the recording system

Date	Time (LT)	H	D	Z	Lightning amplitude (ampere)	Distance (km)	Remark
15-04-2022	23.2 - 24.00	0.1nT	0.2nT	1nT	20968	5.5	GSM90 stopped recording & spikes in HDZ
04-05-2022	7.0 - 8.2	70nT	20nT	150nT	8879, 14243	5.3, 10	Shift in data(HDZ)
29-08-2022	-	-	-	-	37387,24329, 21210, 8553	3.9, 5.5, 9.2, 10	DFM stopped recording
30-04-2017	18.0 - 18.8	0.8nT	1nT	1.2nT	-	-	Spikes in HDZ
26-05-2017	20.5 -23.0	0.2nT	0.2nT	1nT	-	-	Spikes in HDZ

It was suspected that because the new PVR is constructed on the surface and the cables were laid in the surface layer, instead of the vault configuration as in the one which was flooded, the effects of lightning activity on the data has been amplified. Given the fact that in future years more uncertainty and swings in climatic parameters are anticipated due to effects of climate change, it was deemed necessary to conduct further studies to find a location based on optimal ranges of a variety of parameters like topography, distance from MAR lake, the configuration of near surface regolith and saprolite layers along with groundwater conditions.

4. New search for optimal location

Higher ground away from the MAR basin can be found toward the western side of the campus. In order to evaluate its suitability as a new long term location for continuous magnetic measurements, this study aims to delineate the sub-surface structures using the high-resolution magnetic data constrained by resistivity information conducted through Electrical Resistivity Tomography (ERT) and Electrical Vector Resistivity Imaging (EVRI) measurements at the Choutuppal campus and surrounding areas during 2016-2017. The magnetic method can be sensitive to presence of near surface variations and produce a model of these layers as well as in locating faults, folds, shear zones, delineating geological structures, and groundwater contamination studies (Reynolds, 1997; Hinze et al., 2013; Kumar et al., 2018; Dwivedi and Chamoli, 2021, 2022). We try to find out a suitable location for a new SVR (secondary variometer room) where effects of lightning and groundwater level changes can be minimum in the medium-to-long term.

i) 2024 survey

A 1-sec total magnetic field survey was conducted during February 2024 (4 days) at 10 m sampling intervals as same done in 2019 survey. The data of 2019 and 2024 were combined, thus covering a total of ~ 400 × 320 square meters. The diurnal and International Geomagnetic Reference Field (IGRF 14) corrections are applied to the F data, so that the residuals reflect only the local crustal contributions. Finally, we applied the kriging interpolation method to generate the grid and produce the magnetic anomaly of this area (Figure 8a). Further, this was converted by a reduced to equator (RTE) computation to remove ambiguities in location of causative sources of magnetic anomalies, at low and high latitudes. In this study, we chose the values of Delineation=0°, and Inclination=24° and estimate the RTE generated magnetic anomaly map of the study region. The RTE filtered map centres anomalies over their sources and removes the asymmetry of the magnetic anomaly due to nonzero magnetic inclination and helps in magnetic data interpretation (Figure 8b).

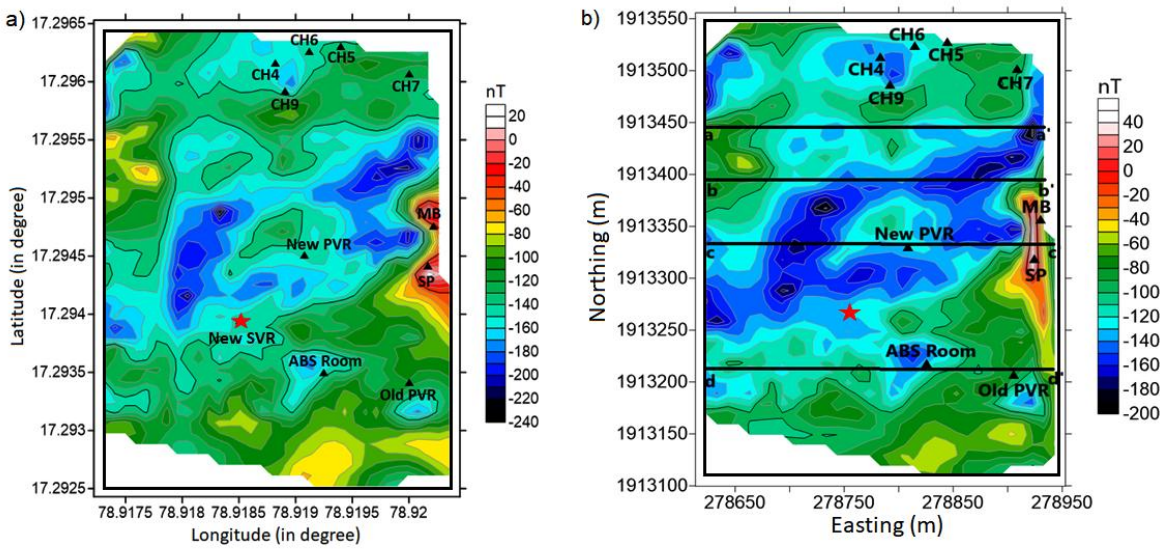

Figure 8: a) The magnetic anomaly of the study area. (MB=main building, SP= solar panel, CH= bore well channels, ABS= absolute, PVR= primary variometer room, SVR= secondary variometer room). Red star mark shows the proposed New SVR in the region, b) the magnetic anomaly after reduced to equator of the study area. The aa', bb', cc' and dd' shows four magnetic profiles modelled.

281 The RTE magnetic anomaly shows a variation of ~ 260 nT in the region. The low
282 anomaly is dominant in the central part followed by the high anomaly near the main
283 building and solar panel. The new PVR lies in the low anomaly region where the three-
284 axis flux magnetometer is installed to record 1-sec H, D, and Z component data of
285 Earth's magnetic field. The ABS room location is set up in the low anomaly zone to
286 measure the Delineation-Inclination using the Mag-01 DI-fluxgate magnetometer
287 mounted on theodolite.
288
289 We have considered four profiles aa', bb, cc', and dd' along EW in the RTE magnetic
290 anomaly map to characterise the subsurface susceptibility model (Figure 8b). The
291 magnetic data shows its importance in characterizing the shallow sub-surface
292 structures, which would be further beneficial for the selection of new location to install
293 magnetic observatory in the campus. The lightning data is considered from the
294 National Remote Sensing Centre (NRSC), Hyderabad, India, to investigate the failure
295 of the DFM (digital fluxgate magnetometer) electronics during the lightning strike. The
296 high-resolution topography data is obtained from the Shuttle Radar Topography
297 Mission (SRTM) Global 30 (https://earthexplorer.usgs.gov/) to plot the elevation of the
298 region.
299
300 The ERT surveys for different profiles (AA', DD', EE', FF' and GG') were carried out
301 using Wenner and Schlumberger arrays with 48 electrodes in the campus. The profiles
302 AA', DD', EE' with 5 m unit electrode spacing achieved a maximum length of 360 m
303 whereas FF' and GG' covers 240 m (Maurya et al, 2021). The vertical cross section
304 along these profiles and a horizontal depth slice at a depth of 30 m below ground level

derived from 3D model reflect few linear conductive features and surficial resistivity heterogeneities (Figure 13a).

ii) Analysis of subsurface source and depths

The fast Fourier transform (FFT), a robust technique is used by several researchers to calculate the mean depth of layered interfaces of the potential field datasets (Chamoli et al., 2011, 2023; Dwivedi et al., 2019). The power spectrum analysis gives the average depth of the sources with an error limit of 10% (Mishra and Pederson, 1982). The 2D radially averaged power spectrum of the RTE magnetic anomaly data shows two linear slope segments corresponding to the average depth of two interfaces around 12±1.2 m and 1±0.1 m (Figure 9).

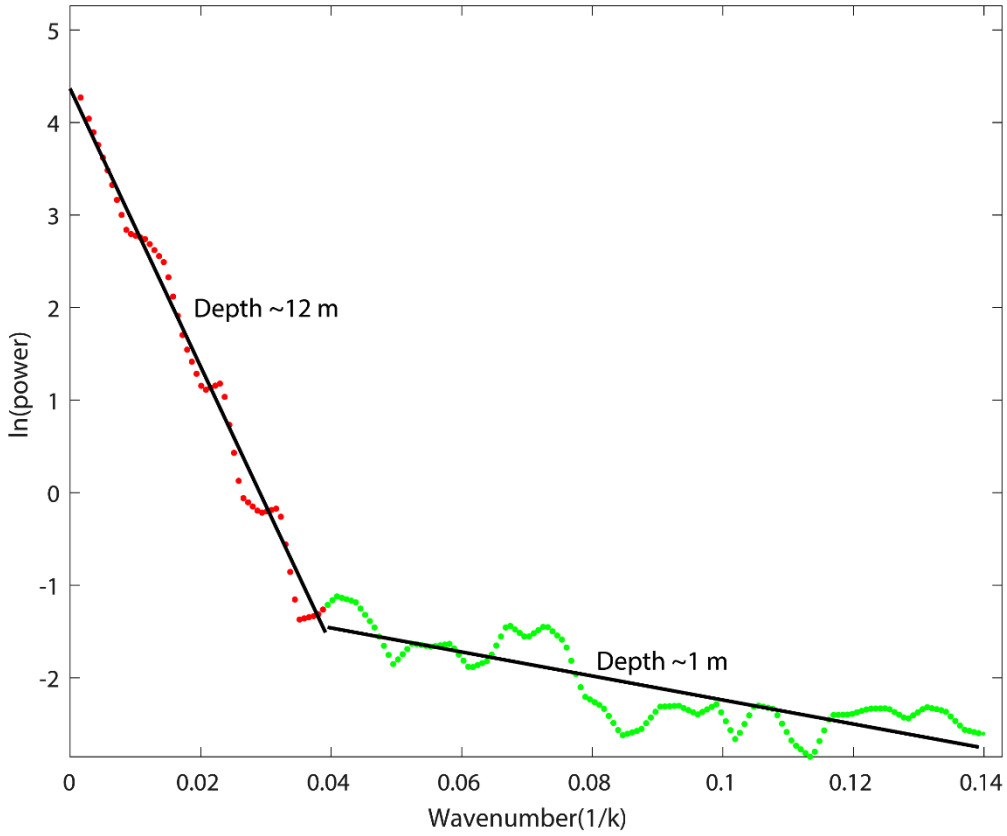

Figure 9: Radially averaged power spectrum of the RTE magnetic anomaly. Different layer segment gives an average depth of layered interfaces.

The tilt depth is an effective method in characterizing the location of source edge as well as magnetic source depth using the tilt angle (TDR) approach (Salem et al., 2007). First, the TDR is described by the following equation (Miller and Singh, 1994).

$$\theta = tan^{-1}\left[\frac{\frac{\partial M}{\partial Z}}{\sqrt{\left(\frac{\partial M}{\partial x}\right)^2 + \left(\frac{\partial M}{\partial y}\right)^2}}\right] \quad (1)$$

where $\frac{\partial M}{\partial x}$, $\frac{\partial M}{\partial y}$, $\frac{\partial M}{\partial z}$ are the first derivative of the magnetic field M in the x, y and z directions. The zero contour (θ =0^0) demarcates the spatial location of magnetic source and tilt amplitudes restrict in the range of +90^0 to -90^0. Salem et al., (2007) introduced the tilt depth technique using the relationship among tilt angle (θ), depth (Z_c), horizontal location (h) of a contact as:

$$\theta = tan^{-1}\left[\frac{h}{Z_c}\right] \quad (2)$$

In the equation 2, the contact location (h =0) lies to the zero values of the contour and depth relates to the horizontal distance between the 0^0 and ±45^0 contour in the TDR map. We apply the technique to generate the tilt angle (TDR), tilt depth solution and histogram plot on the magnetic gridded data. Figure 10 presents the TDR map with displaying of contours of -45°, 0°, +45° (dashed black lines). The TDR shows the short wavelength anomalies and closely spaced contours that corresponds to shallow sub surface sources. The zero contour values of the TDR show the location of the source whereas the half of the distance between ±45° contours demarcates depth of the sources. It can be seen that distance between 0° and +45^0 is demarcated by relative closeness over the shallow sources and wide expanses over the deeper sources.

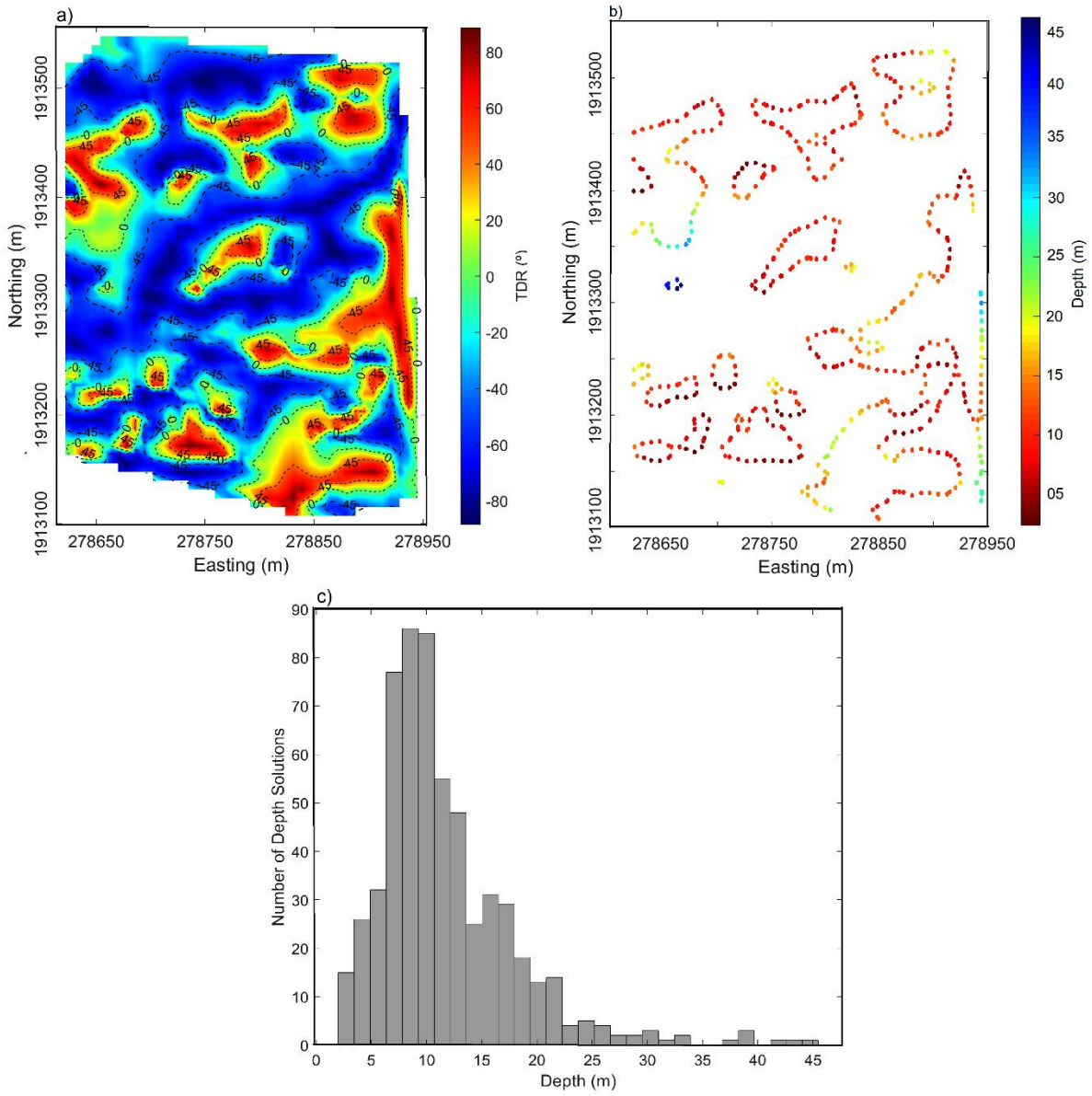

Figure 10: a) The tilt angle plot, b) The tilt depth solutions, c) the tilt depth solution histogram plot of the RTE magnetic anomaly.

The tilt depth solutions of the RTE magnetic anomaly data with depth variation from ~ 2 m to 45 m. Most of the sources lie in shallow depth ~ 2 to 20 m and extended in one direction. The histogram plot shows the variation between number of depth solution and depth (Figure 10c). It is clear from the plot that number of depth solution are maximum in the depth range of ~ 2 m to 20 m which corresponds to shallow source in the sub surface.

iii) Magnetic data inversion and forward models

We invert the RTE magnetic anomaly to estimate the depth variation of the interface with strong susceptibility contrast. We use the method of Parker (1973) which works in the Fourier domain to estimate the depth variation of an undulated interface. The depth of interface can be computed from the magnetic anomaly due to an uneven, uniform magnetized layer by inversion procedure. The method is improved by incorporating high cut filter to ensure the convergence of series and to avoid instability at high wavenumber (Pham et al., 2020). Based on the power spectrum characteristics, we have chosen the cut-off wavenumber between 0.038-0.13 m^{-1} to remove the high frequencies. The resultant map shows that this interface is deepest in the centre of the survey area and shallowest towards the edges; then present PVR and the ABS Room are in the zones where this interface is deep, whereas the old PVR, which was flooded was in the zone of shallow interface (Figure 11a). The calculated depth is inferred as the saprolite layer, which varies from ~ 12 to 16 m with a mean depth of ~14 m. Figure 11b shows the variation of the root mean square (RMS) error against the iteration number. In this case, the inversion process performed 175 iterations, and the RMS error between two successive approximations was reduced from 0.0680 m to 9.9584× 10^{-5} m.

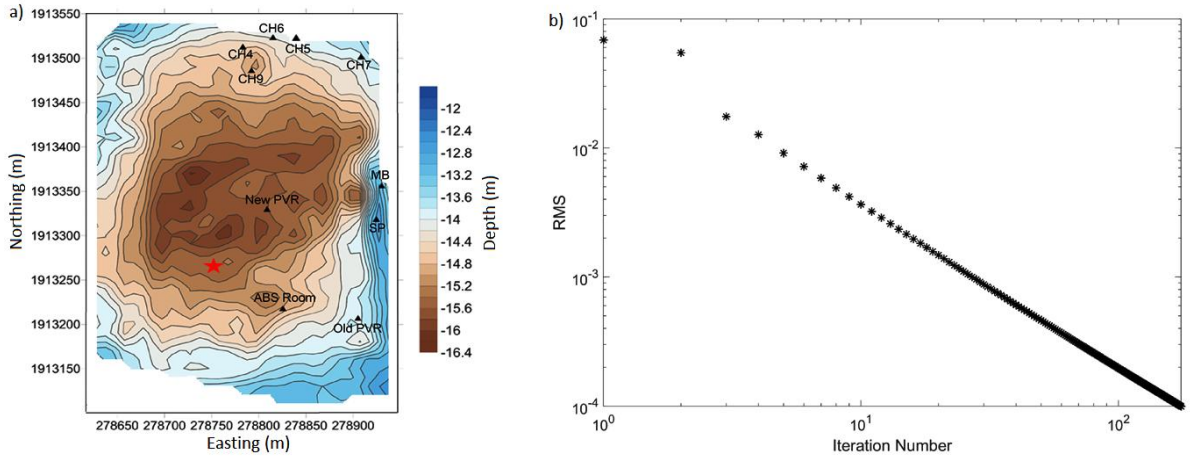

Figure 11: a) The depth variation of the saprolite interface derived from the inversion of the RTE magnetic anomaly after removing the high frequency component, b) variation of RMS error against the iteration number.

Further, we model the RTE derived magnetic anomaly data along four profiles aa', bb', cc', and dd' (Figure 8b) to delineate the details of the sub-surface structures. The forward modelling along these profiles is carried out using the IGMAS+ software, a tool for forward and inverse modelling of potential field datasets (Anikiev et al., 2023). The total length of theses profiles are ~310 m which show the depth variations up to 50 m from the surface (Figure 12a). The 2D models along these profiles explains the presence of three layered structures from the surface up to a depth of 50 m as: sandy regolith (~0.3 susceptibility in SI), saprolite (~3 susceptibility in SI), and fissured granite (~2.5 susceptibility in SI). The average susceptibility value for sandy regolith layer is measured in the field using KT-10 magnetic susceptibility meter whereas others are referenced from Telford et al., (1990). The saprolite interface is incorporated in the models based on previous results of ERT data (Nicolas et al., 2019). The average thickness of the sandy regolith layer is ~3 m whereas the saprolite layer is ~ 10 m in the models. Both the saprolite and regolith layers show undulations in the all models.

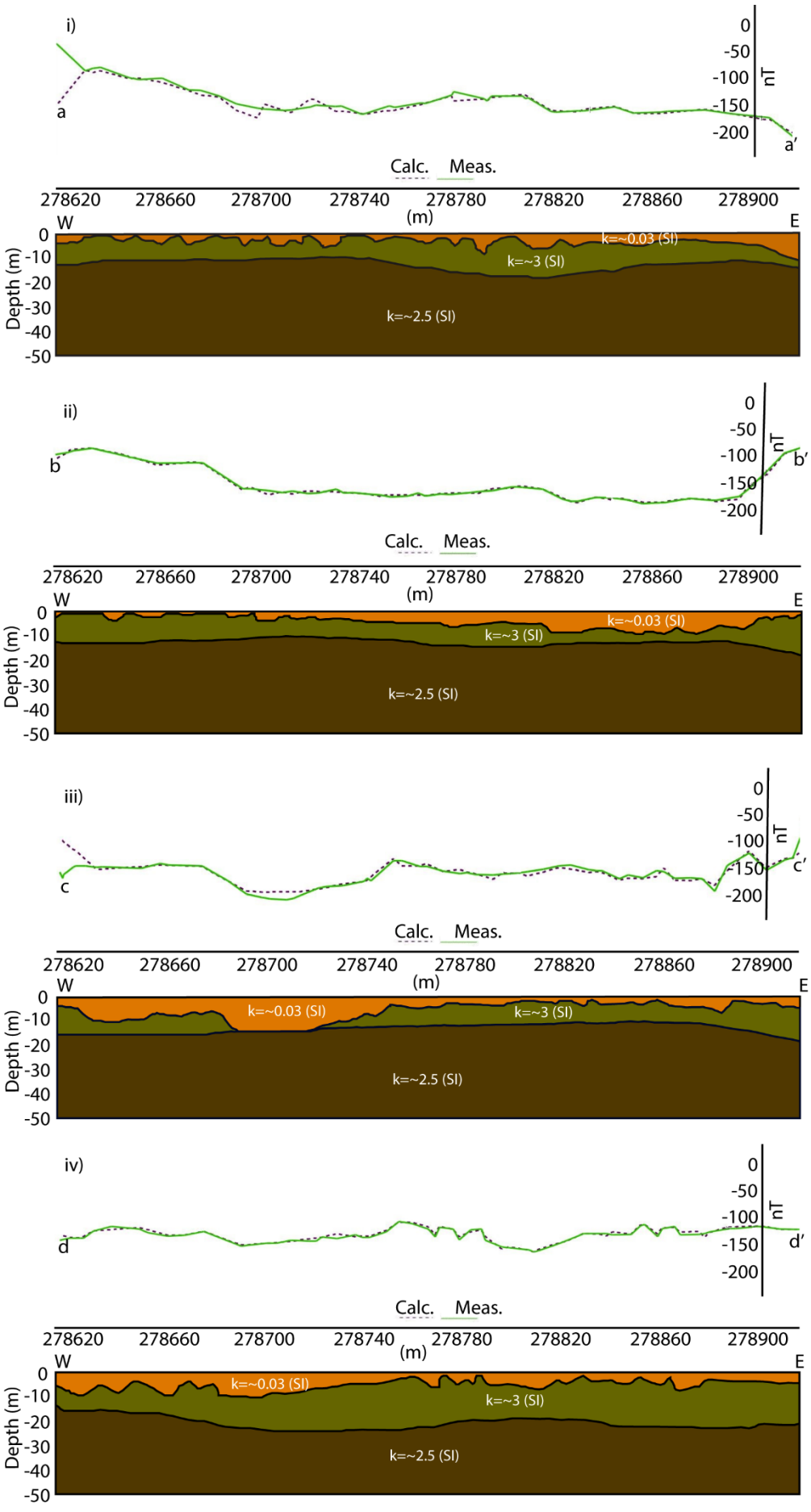
i)
a
a′
0
-50
-100
-150
-200
nT
Calc.
Meas.
278620
278660
278700
278740
278780
278820
278860
278900
W
(m)
E
Depth (m)
0
-10
-20
-30
-40
-50
k=~0.03 (SI)
k=~3 (SI)
k=~2.5 (SI)
ii)
b
b′
iii)
c
c′
iv)
d
d′

401

Figure 12: Magnetic data modelling across the profiles i) aa', ii) bb', iii) cc' and iv) dd' incorporating constrain from power spectrum, and past ERT studies. Top, middle and bottom layers in the models are sandy regolith, saprolite and granitic basements. The marked arrows show the location of New and Old PVR in profile cc' and dd'.

iv) Correlation with conductivity data/information

The cc' magnetic profile is close to the vertical resistive cross-section along AA' of Maurya et al., (2021) where resistivity increases from surface to depth (Figure 13a). The old surface and apparent resistivity data of the region is digitized from the Sanker Narayan et al., (1967) and overlaid over the topography (Figure 13b, 13c). The apparent resistivity shows lateral varying high resistivity outward and vice-versa inside the Choutuppal campus (Figure 13b). This indicates that conductivity decreases outward, highlighting the presence of conductive soil layers within the campus.

The calculated saprolite depth by inverting magnetic data at different locations are ~ 15.5 m (new PVR), ~ 15 m (ABS Room and CH9), ~ 13 m (MB and SP), ~14 m (old PVR, CH5, CH6, CH7), ~ 14.5 m (CH4) (Figure 11a). Whereas, depth estimation by the ERT data are ~ 13.5 m (new PVR), ~ 18 m (ABS Room), ~ 15 m (CH9), ~ 14 m (MB, SP and CH4), ~22 m (old PVR and CH6), ~ 29 m (CH5) ~ 17 m (CH7) respectively (Figure 13d). The calculated depth from these two different datasets show a discrepancy of ~ 2m except at the locations of CH5, CH6 and old PVR. The ERT survey estimates the upper fissured layer depth (~ 9 to 33 meters) of the Choutuppal campus and shows the undulated interface creating compartmentalised aquifers (Nicolas et al., 2019).

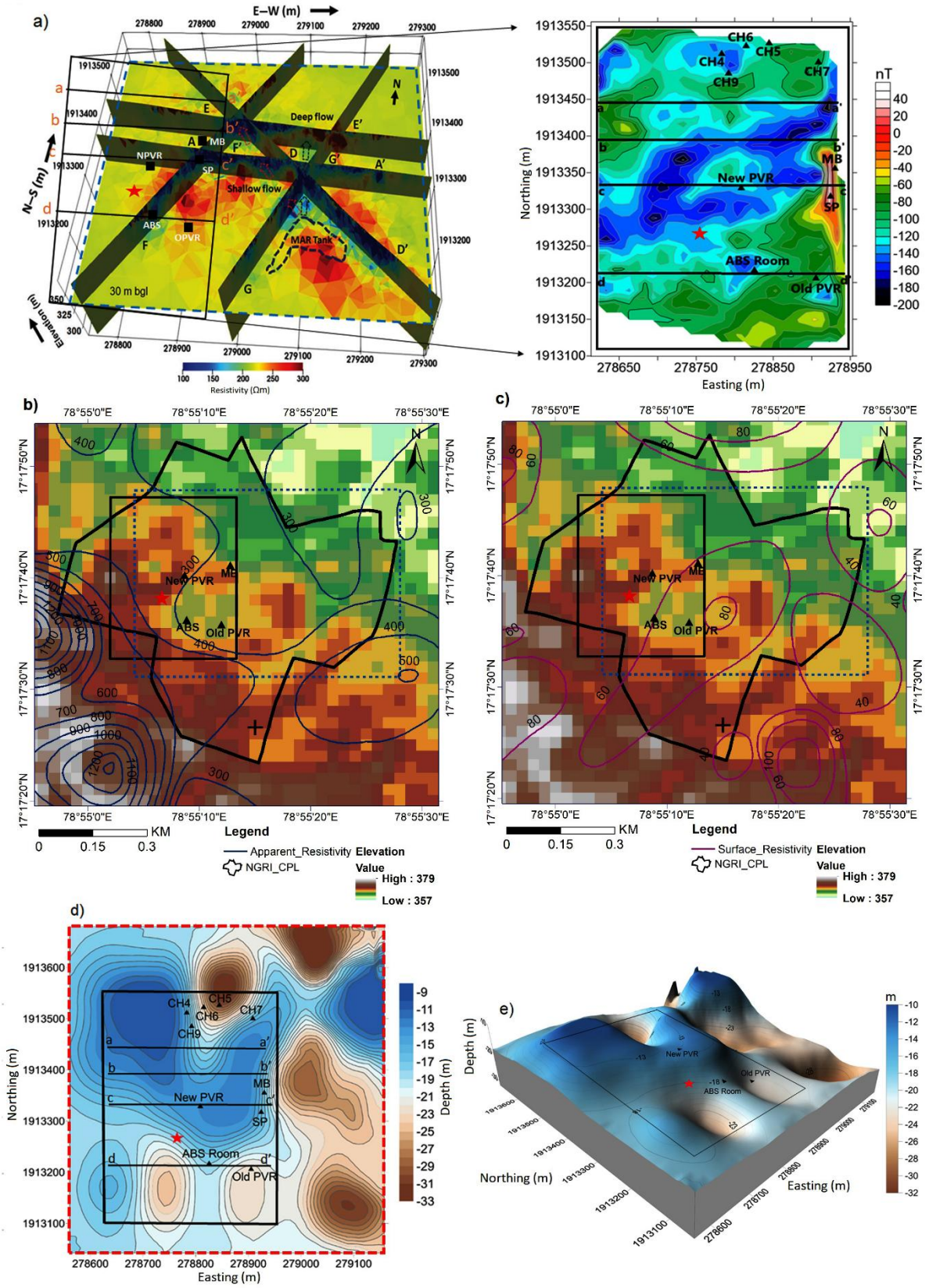

430

431 **Figure 13:** a) A resistivity model of the 2019 profiles along AA', DD', EE', FF', and GG'
432 and a depth slice at 30m below ground level (after Maurya et al., 2021), b) apparent
433 resistivity, c) surface resistivity superimposed over the topography with lightning strike

location (+ symbol, intensity of 23208 ampere at a distance of 400 m from the MB on 04th May, 2022), d) depth estimation of saprolite interface from ERT data (after Nicolas et al., 2019), e) 3D view of saprolite interface. The blue and red dotted rectangles represent the areas corresponding to the resistivity model and the saprolite interface, respectively, while the black rectangle highlights the magnetic anomaly region.

5. Discussion and conclusion: proposed optimal location for SVR

The high resolution magnetic data provide a detailed shallow sub-surface structure at the CPL observatory. The power spectrum result shows two segments at a depth of ~ 12 m and ~1 m corresponding to saprolite and sandy regolith interface. These depths are similar to the previous depth estimated using the drilling data by Dewandel et al., (2006). The inversion results show the depth variation of the saprolite interface ~ 12 to 16 m (Figure 11a) which underestimate with the upper fissured layer depth from the ERT survey (Figure 13d). The obtained interface shows depression in the central region of the map with crests in the outer region and linear variation in depths (Figure 11a). The estimated depths at different locations shows ~ 2 m differences from these two datasets except at the location of CH5, CH6 and old PVR. These discrepancies in the depths estimation may be due to measurements of two different independent physical parameters susceptibility and conductivity. The saprolite interface might be delineate better by the ERT data due to presence of significant resistivity contrast between saprolite and granitic bedrock in the region (Robinson et al., 2008; Gourdol et al., 2021). The tilt depth plot of the anomaly data reflects depth variation from ~ 2 m to 45 m (Figure 10b). The histogram plot confirms the presence of the shallow sources in the depth range of ~ 2 m to 20 m based on the majority of a number of depth solutions (Figure 10c). These shallow sources are in circular and elongated shapes which may be residue of igneous intrusion (Gorczyk and Vogt, 2018). At shallow depths, circular bodies with a magnetic contact source might produce symmetric

anomalies in the magnetic data (Hinze et al., 2013). In contrast, elongated bodies may produce linear magnetic anomalies that follow the direction of the body as in the present study.

The sub-surface susceptibility models along the magnetic profiles aa', bb', cc', and dd' reflect the geometry of sandy regolith, saprolite layer and basement fissured granite (Figure 12). The saprolite layer shows undulating variation with quiet thick and thin at different locations along the profiles. These variations illustrate that the saprolite layer is thin in the region where the anomaly is low and it shows the thickness in the region where the anomaly is high. The magnetic anomaly shows a large depression of length ~ 80 m in the profile cc' where saprolite layer is absent and this depression arises due to sandy layer in the model. The 3D cross-sectional resistivity model infers the presence of high conductive anomalies followed by the moderate conducting saprolite layer and the low conductive basement rocks (Figure 13a).

Figure 13b shows that the apparent resistivity increases laterally outward, indicating the presence of highly conductive soil layers within the campus (Sanker Narayan et al., 1967). The apparent and surface resistivity demonstrate the linear relationship with the topography. The comparison between the latest resistivity model (~200 Ωm variation) for 2019 profiles (Figure 13a) and the old apparent resistivity (~300 Ωm variation) plot in 1964 (Figure 13b) shows the resistivity change of ~100 Ωm. This discrepancy may be due to the presence of newly constructed artificial recharge pond which may decrease the resistivity due to its high conductive nature. The thin saprolite layer may be associated with high electrical conductivity, which can result in a low magnetic anomaly, and vice versa. Overall, the resistivity variation increases from

surface to greater depth. The resistivity model also show that the artificial recharge pond has good subsurface connectivity, helping the groundwater recharge towards the north and northwest directions in the campus (Maurya et al., 2021). The water level started to rise in June-2016 and reached to very shallow depth in channels during December 2017. It is evident that since last half of 2016, the recharge has led to saturation, which transformed the hydrogeological regime of the campus. This may also cause a partial change in the rock magnetism due to water saturation (Csontos et al., 2019) resulting in a decrease in the magnetic anomaly (Figure 4a, 8a). The rainfall of 2017 monsoon combined with the already prevalent saturated conditions led to the flooding of the magnetometer vault. The location of new PVR has advantages as it is away from the water recharge pond, minimal magnetic anomaly but generation of induced current in the rainy seasons due to presence of conductive environment around the location. The effect of lightning strikes on the data with increasing distance, intensity and ground conductivity shows that higher intensity strikes has had an impact of the data and instruments.

Based on the above it is very crucial to determine the location and configuration where the installation can avoid the effects of groundwater fluctuations as well as lightning strikes, based on the nature of subsurface rocks, soil conditions, and their magnetic variations. The susceptibility model along with resistivity information are used to make a selection of a new SVR (78.9185E, 17.2939N), indicated by red star in Figures 1, 8, 11, 13. This location is on low magnetic anomaly of ~ -145 nT (Figure 8a), resistivity ~200 Ωm (Figure 13a), moderately high ground ~367 m (Figure 13b), and depth of saprolite layer ~ 20 m (Figure 13d). A thicker saprolite layer can enhance the resistive environment and reduce current propagation. The location's sufficient distance (~ 320

m) from the recharge tank ensures that water infiltration is unlikely to pose a significant issue. It is proposed that the pillar will be constructed within a semi-underground vault, in order to minimize the influence of induced currents during rainy seasons and lightning strikes. Additionally, the volume surrounding the pillar should be filled using high-resistivity material, such as Quartzite, to further minimize the likelihood of induced currents during lightning events or wet conditions.

Acknowledgements:

We thank the Director, NGRI, for supporting the work; reference no. NGRI/Lib/2025/Pub-35. The authors are thankful to Dr. Subhash Chandra and other colleagues from the ground water department of CSIR-NGRI for providing the bore well water level data and resistivity results. We also thank Dr. Phani Chandrasekhar, Dr. Rahul Prajapati and Dr. L. Manjula for help towards the repeat surveys.

Authors' contributions:

DD: Conceptualization, Methodology, Computation and Modeling, Formal analysis, Writing-original draft and editing

SY: Data Processing, Modeling

KA: Conceptualization, Validation, Review and final editing

RM: Lightning data analysis, maps and figures

AT: Lightning data, validation

Declaration of Competing Interest:

The authors declare that they have no competing financial interests or personal relationships that could have appeared to influence the work reported in this paper.

Funding:

No funding was provided for this work.

Availability of data and material

The magnetic data associated with this research are available and can be obtained upon the request from corresponding author. The topography data is obtained from the Shuttle Radar Topography Mission (SRTM) Global 30 (https://earthexplorer.usgs.gov/). The lightning data can be accessed through the ISRO - National Remote Sensing Centre, Hyderabad (https://bhuvan-app1.nrsc.gov.in/lightning/).

References:

Anikiev, D., Götze, H.-J., Plonka, C., et al., 2023. IGMAS+: Interactive Gravity and Magnetic Application System. GFZ Data Services. https://doi.org/10.5880/GFZ.4.5.IGMAS.

Arora K., Chandrashakhar Rao K., Manjula L., et al., 2016. The new magnetic observatory at Choutuppal, Telangana, India. Journal of Indian Geophysical Union, Special volume-2, 67-75.

Arora K., Selles A., Manjula L., et al., 2017. CPL Magnetic Observatory: Groundwater flooding and Relocation requirement. Technical Report No. NGRI-magObs-2017-946.

Chamoli A., Pandey A.K., Dimri V.P., et al., 2011. Crustal configuration of the northwest Himalaya based on modeling of gravity data. Pure and Applied Geophysics 168 (5), 827–844.

563 Chamoli A., Rana S.K., Dwivedi D., et al., 2023. Crustal structure and fault geometries
564 of the Garhwal Himalaya, India: Insight from new high-resolution gravity data modeling
565 and PSO inversion. Tectonophysics, 859, 229904.
566 https://doi.org/10.1016/j.tecto.2023.229904.
567 Csontos A., Kónya P., Falus G., et al., 2019. Unstable spatial differences of the
568 geomagnetic elements caused by changing water saturation of a volcanic
569 sediment. Annals of Geophysics, 61(6), GM669. https://doi.org/10.4401/ag-7351
570 Dewandel B., Lachassagne P., Wyns R., et al., 2006. A generalized 3-D geological and
571 hydrogeological conceptual model of granite aquifers controlled by single or
572 multiphase weathering. Journal of Hydrology, 330, 260-284,
573 https://doi.org/10.1016/j.jhydrol.2006.03.026.
574 Dewandel B., Maréchal J.C., Bour O., et al., 2012. Upscaling and regionalizing
575 hydraulic conductivity and effective porosity at watershed scale in deeply weathered
576 crystalline aquifers. Journal of Hydrology, 416–417, 83-97.
577 https://doi.org/10.1016/j.jhydrol.2011.11.038.
578 Dwivedi D., Chamoli A., Pandey A.K., 2019. Crustal structure and lateral variations in
579 Moho beneath the Delhi fold belt, NW India: Insight from gravity data modeling and
580 inversion. Physics of the Earth and Planetary Interiors, 297, 106317.
581 https://doi.org/10.1016/j.pepi.2019.106317
582 Dwivedi D., Chamoli A., 2021. Source Edge Detection of Potential Field Data Using
583 Wavelet Decomposition. Pure and Applied Geophysics,
584 https://doi.org/10.1007/s00024-021-02675-5.
585 Dwivedi D., Chamoli A., 2022. Seismotectonics and lineament fabric of Delhi fold belt
586 region, India. Journal of Earth System Science, 131, 74.
587 https://doi.org/10.1007/s12040-022-01829-w.

588 Gorczyk W., Vogt K., 2018. Intrusion of magmatic bodies into the continental crust:
589 3D numerical models. Tectonics, 37, 705–723. https://doi.org/10.1002/2017TC004738
590 Gourdol L., Clément R., Juilleret J., et al., 2021. Exploring the regolith with electrical
591 resistivity tomography in large-scale surveys: electrode spacing-related issues and
592 possibility. Hydrology and Earth System Sciences, 25, 1785–1812,
593 https://doi.org/10.5194/hess-25-1785-2021, 2021.
594 Guihéneuf N., Boisson A., Bour O., et al., 2014. Groundwater flows in weathered
595 crystalline rocks: Impact of piezometric variations and depth-dependent fracture
596 connectivity. Journal of Hydrology, 511, 320–334.
597 https://doi.org/10.1016/j.jhydrol.2014.01.061.
598 Hinze W.J., Von Frese R.R.B., Von Frese R., et al., 2013. Gravity and Magnetic
599 Exploration: Principles, Practices, and Applications. Cambridge University Press,
600 Cambridge.
601 Kumar R., Bansal A. R., Anand S. P., et al., 2018. Mapping of magnetic basement in
602 Central India from aeromagnetic data for scaling geology. Geophysical Prospecting,
603 66, 226–239.
604 Maréchal J. C., Selles A., Dewandel B., et al., 2018. An observatory of groundwater in
605 crystalline rock aquifers exposed to a changing environment: Hyderabad, India.
606 Vadose Zone Journal, 17, 180076, https://doi.org/10.2136/vzj2018.04.0076
607 Maurya V.P., Chandra S., Sonkamble S., et al., 2021. Electrically inferred subsurface
608 fractures in the crystalline hard rocks of an Experimental Hydrogeological Park,
609 Southern India. Geophysics, 86(5), WB9-WB18, https://doi.org/10.1190/geo2020-
610 0327.1
611 Miller H. G., Singh V., 1994. Potential field tilt-a new concept for location of potential
612 field sources. Journal of Applied Geophysics, 32, 213–217.

613 Mishra D., Pedersen L.B., 1982. Statistical analysis of potential fields from subsurface
614 reliefs. Geoexploration, 19, 247–265. https://doi.org/10.1016/0016-7142(82)90030-8.
615 Nicolas M., Bour O., Selles A., et al., 2019. Managed Aquifer Recharge in fractured
616 crystalline rock aquifers: Impact of horizontal preferential flow on recharge dynamics.
617 Journal of Hydrology, 573, 717-732, https://doi.org/10.1016/j.jhydrol.2019.04.003.
618 Parker R., 1973. The rapid calculation of potential anomalies. Geophysical Journal
619 International, 31 (4), 447-455, https://doi.org/10.1111/j.1365-246X.1973.tb06513.x
620 Pham L.T., Oksum E., Gómez-Ortiz D., et al., 2020. MagB_inv: A high performance
621 Matlab program for estimating the magnetic basement relief by inverting magnetic
622 anomalies. Computers & Geosciences, 134,104347,
623 https://doi.org/10.1016/j.cageo.2019.104347
624 Reynolds J., 1997. An Introduction to Applied and Environmental Geophysics, Wiley,
625 Chester, 2nd edition, 710p.
626 Robinso D. A., Binley A., Crook N., et al., 2008. Advancing process-based watershed
627 hydrological research using near-surface geophysics: A vision for, and review of,
628 electrical and magnetic geophysical methods, Hydrological Processes, 22, 3604–
629 3635, 2008.
630 Salem A., Williams S., Fairhead J., et al., 2007. Tilt-depth method: a simple depth
631 estimation method using first-order magnetic derivatives. Leading Edge 26, 1502–
632 1505.
633 Sanker Narayan, 1964. Establishment of a magnetic observatory at NGRI. Bull NGRI,
634 2, 115-122.
635 Sanker Narayan P.V., Ramanujachary K.R., Sarma S.V.S., et al., 1967. Establishment
636 of a geoelectric observatory by the NGRI, Hyderabad, at Choutuppal, Nalgonda, Bull.
637 NGRI, 5, 155.

638 Sarma Y.S., Sanker Narayan P.V., Ramanujachary K.R., et al., 1969. Three component
639 induction magnetometer for recording geomagnetic micropulsations at the Geoelectric
640 observatory at Choutuppal, Bull. NGRI, 7, 51-65.
641 Spector A., Grant F.S., 1970. Statistical models for interpreting aeromagnetic data.
642 Geophysics 35 (2), 293–302.
643 Svendsen K.L., Davis W.M., McLean S.J., Meyers, H. 1990. A report on geomagnetic
644 observatory operations. NOAA, NGDC, Boulder, Colorado, USA.
645 Taori A., Suryavanshi A., Pawar S., et al., 2022. Establishment of lightning detection
646 sensors network in India: generation of essential climate variable and characterization
647 of cloud-to-ground lightning occurrences. Natural Hazards, 111, 19-32,
648 https://doi.org/10.1007/s11069-021-05042-8
649 Taori A., Suryavanshi A., Bothale R.V., 2023. Cloud-to-ground lightning occurrences
650 over India: seasonal and diurnal characteristics deduced with ground-based
651 lightning detection sensor network (LDSN). Natural Hazards, 116, 4037-4049.
652 https://doi.org/10.1007/s11069-023-05839-9
653 Telford W. M., Geldart L. P., Sheriff R. E., 1990. Applied Geophysics (2nd ed.).
654 Cambridge: Cambridge University Press.
655 Tiwari V.M., Vyghreswara Rao M.B.S., Mishra D.C., et al., 2006. Crustal structure
656 across Sikkim, NE Himalaya from new gravity and magnetic data. Earth and Planetary
657 Science Letters, 247, 61-69, https://doi.org/10.1016/j.epsl.2006.03.037.